Polyhedron 33 (2012) 450–455

Contents lists available at SciVerse ScienceDirect

Polyhedron

journal homepage: www.elsevier.com/locate/poly

Lead hexacyanoferrate(II) tetrahydrate: Crystal structure, FTIR spectroscopy and thermal decomposition studies

Diego M. Gil [a], Manuel Avila [b], Edilso Reguera [b], Silvina Pagola [c,d], M. Inés Gómez [a], Raúl E. Carbonio [e,*,1]

[a] Instituto de Química Inorgánica, Facultad de Bioquímica, Química y Farmacia, Universidad Nacional de Tucumán, Ayacucho 471, 4000, San Miguel de Tucumán, Argentina
[b] Centro de Investigación en Ciencia Aplicada y Tecnología Avanzada del IPN, Unidad Legaria, México D.F., Mexico
[c] Applied Research Center, 12050 Jefferson Avenue, Newport News, VA 23606, USA
[d] College of William and Mary, Department of Applied Science, McGlothlin-Street Hall 314, Williamsburg, VA 23185, USA
[e] Instituto de Investigaciones en Fisicoquímica de Córdoba (INFIQC) – CONICET, Departamento de Fisicoquímica, Facultad de Ciencias Químicas, Universidad Nacional de Córdoba, Ciudad Universitaria, X5000HUA Córdoba, Argentina

ARTICLE INFO

Article history:
Received 23 August 2011
Accepted 9 December 2011
Available online 16 December 2011

Keywords:
$Pb_2[Fe(CN)_6]\cdot 4H_2O$
Crystal structure
Synchrotron
PXRD
Thermal decomposition

ABSTRACT

$Pb_2[Fe(CN)_6]\cdot 4H_2O$ was synthesized by mixing aqueous solutions of lead(II) nitrate and potassium ferrocyanide. Its crystal structure was solved *ab initio* from synchrotron powder X-ray diffraction data using the direct methods and refined by the Rietveld method. Thermal analysis (TGA and DTA), Fourier Transform Infrared Spectroscopy (FTIR) and scanning electron microscopy (SEM) studies were also used for the solid state characterization of this compound and its decomposition products. The complex crystallizes in the monoclinic crystal system, space group $P2_1/n$. The Fe^{2+} cation is octahedrally coordinated to six cyano groups, and the Pb^{2+} cation is penta-fold coordinated to three N atoms from C≡N ligands and two O atoms from coordinated water molecules. The most important peculiarity of the structure of this complex is the occurrence of water bridges linking two neighboring Pb^{2+} cations. An unusual Fe–C≡N–$Pb(H_2O)_2$–Pb–N≡C–Fe linkage alternates with a usual Pb–N≡C–Fe one. Zeolitic water molecules are also observed in the structure; they are located in small channels in the structure and they are hydrogen bonded to coordinated water molecules forming a cumulus. Coordinated water and zeolitic water molecules in this complex can be removed without affecting the hexacyanometallate framework. The thermal decomposition in air to produce $Pb_2Fe_2O_5$ and PbO as final products has been studied by thermogravimetric and differential thermal analysis, FTIR spectroscopy and laboratory powder X-ray diffraction. The crystallite size and morphology of the complex and its thermal decomposition products were evaluated by SEM.

1. Introduction

A number of previous studies confirmed the existence of hexacyanoferrates of heavy representative elements of the group IVA, but data of the structure and properties of these compounds are not available. Recently, Zubkov et al. have synthesized anhydrous Pb^{2+} and Sn^{2+} hexacyanoferrates(II) [1]. X-ray and neutron diffraction investigations revealed that the $Pb_2[Fe(CN)_6]$ and $Sn_2[Fe(CN)_6]$ phases crystallize in a trigonal crystal system, space group $P\bar{3}$, $Z = 1$ [1] but there are not structural information about their hydrates. These compounds belong to the group of cyanometallate complexes of the type $T_2[Fe^{II}(CN)_6]\cdot xH_2O$ (where T is a transition metal cation). The majority of these compounds posses good ion-exchange properties (the ability of transition metal cations involved in the first coordination sphere of the complexes to exchange with heavy univalent alkali metal ions in solutions), which makes them good as inorganic sorbents [2]. Owing to their high Curie temperatures, the main group metal and transition metal hexacyanoferrates can be also used as precursors for designing three-dimensional molecular magnets with controlled magnetic moments [3–5].

The metal centers in hexacyanometallates are usually bridged by C≡N groups, where the C and N ends are linked to only one metal. The metal M linked at the C end always adopts octahedral coordination forming the anionic hexacyanometallate octahedral block, $[M^n(CN)_6]^{6-n}$. The 3D framework is formed when neighboring blocks are linked at their N ends through a second transition metal (T) [3]. The C≡N ligand has the ability to serve as bridge group between neighboring metal centers, removing electron density from the M metal linked at its C end through a π back-bonding interaction, to increase the charge density on the N end that is the coordination site for the T metal. This leads to the overlap of the electron clouds of neighboring metal centers and to their spin coupling, and thereby a magnetic ordering can be established. This

* Corresponding author. Tel.: +54 351 433 4180x127; fax: +54 351 433 4188.
E-mail address: carbonio@fcq.unc.edu.ar (R.E. Carbonio).
[1] Member of the Research Career of CONICET.

0277-5387/$ - see front matter © 2011 Elsevier Ltd. All rights reserved.
doi:10.1016/j.poly.2011.12.006

supports the role of hexacyanometallates as prototype of molecular magnets [4]. It is known that the magnetic ordering of hexacyanoferrates is associated with the indirect exchange interactions through C≡N groups [2,5], whereas the Fe^{+2}–Fe^{+2} direct interactions are absent, because the distances between the nearest neighbor iron ions are usually larger than 6 Å. The magnetic interactions between $Fe(CN)_6$ octahedra occur through a T magnetic ion according to the scheme –M–C–N–T–N–C–M– where T = Fe, Co, Ni, Cr and Mn [6].

The heteronuclear complexes of the type $A[MM'(CN)_6]\cdot xH_2O$ (A = lanthanide, Y, alkaline earth metal or Bi; M,M′ = transition metals) have been extensively studied as precursors of perovskite-type oxides $AMM'O_{3-\delta}$ [7–11]. The thermal decomposition of heteronuclear hexacyano-complexes is a promising method for the preparation of homogeneous mixed oxides on atomic level at low temperatures compared with the conventional ceramic method [7–11]. The use of a precursor containing the appropriate A/B ratio enforces the formation of ABO_3 perovskites with the precise stoichiometry, thus controlling and preventing any elements segregation generally observed in conventional methods and allowing the synthesis of the desired mixed oxide at very low temperatures [8]. The oxides so prepared have relatively high specific surface areas and consequently can be used as catalysts in different reactions [12].

Perovskite-type oxides of general formula ABO_3 containing Bi^{3+} and Pb^{2+} at the A positions are interesting in view of their potential ferroelectricity [13,14] and multiferroism, such as in $BiCrO_3$ and $BiFeO_3$ [17,18]. This is mainly due to either the stereochemical effect of the $6s^2$ lone-pair of electrons or the covalent A–O bonds (A = Bi or Pb), that stabilize distorted acentric structures [15,16] generating permanent electric dipoles (ferroelectricity). Taking these observations into account, the preparation and study of perovskite materials that have both, a cation containing lone-pair of electrons as well as a magnetic ion located at the A and/or B perovskite sites is a design strategy to obtain new multiferroic and ferroelectric compounds. Recently, Abakumov et al. has prepared $Pb_2Fe_2O_5$, a perovskite based structure with an incommensurate superstructure [19,20] and Wang and Tan have prepared this compound by sol–gel synthesis reporting multiferroic properties [21].

In the present article, we have solved *ab initio* and refined the crystal structure of $Pb_2[Fe(CN)_6]\cdot 4H_2O$ using synchrotron powder X-ray diffraction (SPXRD) and complemented this study with FTIR spectroscopy. We also have studied its decomposition process to produce $Pb_2Fe_2O_5$ and PbO using FTIR spectroscopy, thermogravimetric and differential thermal analysis (TGA and DTA, respectively) and laboratory powder X-ray diffraction (PXRD).

2. Experimental

$Pb_2[Fe(CN)_6]\cdot 4H_2O$ was prepared by mixing equal volumes of 0.2 M $Pb(NO_3)_2$ and 0.1 M $K_4[Fe(CN)_6]$ aqueous solutions and stirred for 2 h. The white precipitate obtained was filtered, washed several times with distilled water and dried in vacuum until constant weight was achieved. The solid state properties of the obtained material were studied with energy-dispersed spectroscopy (EDS) analysis, SXRPD and FTIR spectroscopy. The degree of hydration and thermal stability of $Pb_2[Fe(CN)_6]\cdot 4H_2O$ were studied by using TGA and DTA. The metal atomic ratio found from EDS analysis was close to 2:1 and agrees with the expected formula unit $Pb_2[Fe(CN)_6]\cdot 4H_2O$.

TGA and DTA curves were obtained from a Shimadzu TGA/DTA-50 balance in the temperature range 20–800 °C at a heating rate of 5°/min under flowing air. FTIR spectra (in the region 4000–400 cm^{-1}) were recorded at room temperature (RT) using KBr pellets, on a FTIR Perkin Elmer 1600 spectrophotometer in the transmission mode.

The high resolution SXRPD data for the structure solution and refinement of $Pb_2[Fe(CN)_6]\cdot 4H_2O$ was collected at room temperature at the X16C X-ray powder diffraction beamline of the NSLS, Brookhaven National Laboratory. The wavelength was 0.699204 Å. The diffraction data was collected between 2θ 1.000° and 43.5430° with 0.003° step size and counting time 1 s per step. The SXRPD pattern was indexed using the program DICVOL [22]. The crystal structure of $Pb_2[Fe(CN)_6]\cdot 4H_2O$ was solved *ab initio* by direct methods using the program SHELXS [23] from the extracted intensities according to the Le Bail method [24]. The structure solution procedure was carried out for all the probable space groups. The structural refinement was performed by using the Rietveld method [25] with the program FULLPROF [26], using the pseudo-Voigt peak shape function. No angular regions were excluded and the following parameters were refined: zero-point, scale factor, pseudo-Voigt parameters of the peak shape, full-width at half-maximum, positional, isotropic thermal displacement parameters and unit cell parameters.

Laboratory PXRD profiles of the thermal decomposition products at different temperatures were obtained at RT in a PANalytical X-Pert Pro X-ray powder diffractometer with Cu Kα radiation, between 5° and 90° in 2θ in steps of 0.02° and counting time of 1 s per step.

Based on TGA results, the complex $Pb_2[Fe(CN)_6]\cdot 4H_2O$ was heated in a furnace at different temperatures in air. The sample was introduced into the furnace and heated from RT at 5°/min to the desire temperature, which was then maintained for 6 h. After that, it was cooled to RT at 5°/min.

The size and morphology of the particles were determined by scanning electron microscopy (SEM) in a ZEIS SUPRA-55 VP instrument, and the chemical compositions of the powders were determined with an Oxford INCA PentaFet X3 energy dispersive (EDS) X-ray analyzer.

3. Results and discussion

3.1. FTIR spectroscopy

The FTIR spectrum of the complex $Pb_2[Fe(CN)_6]\cdot 4H_2O$ has three absorption bands associated with the C≡N ligands: ν(C≡N), δ(M–C≡N) and ν(M–C) and absorption bands due to coordinated and zeolitic water: ν(OH), δ(HOH), $\rho_r(H_2O)$, $w(H_2O)$. Fig. 1 shows the FTIR spectra of $Pb_2[Fe(CN)_6]\cdot 4H_2O$ and $Pb_2[Fe(CN)_6]$. The stretching vibration of the C≡N ligands appears as a single absorption at 2041 cm^{-1} indicating that all C≡N bonds are equivalents. The δ(M–C≡N) and ν(M–C) vibrations appear at 592 and 430 cm^{-1}, respectively. These vibrations are observed in the frequency values

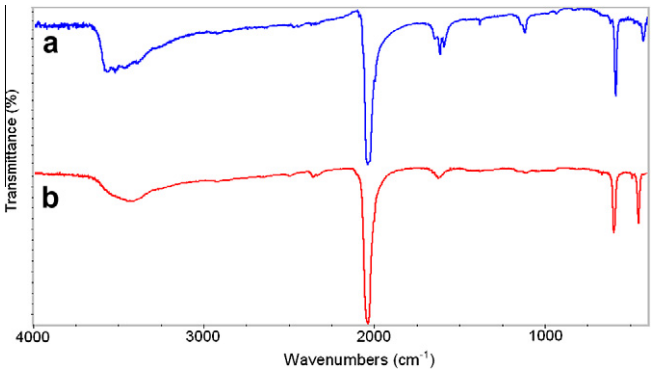

Fig. 1. FTIR spectra of (a) $Pb_2[Fe(CN)_6]\cdot 4H_2O$ and (b) anhydrous $Pb_2[Fe(CN)_6]$.

expected for hexacyanometallates(II) [27]. The two narrow bands at 3570 and 3524 cm^{-1} can be assigned to the O–H stretching of coordinated water. The two broad stretching bands observed at 3466 and 3387 cm^{-1} are due to zeolitic water. The highest frequency band in the δ(HOH) region, at 1646 cm^{-1}, corresponds to the weakly bonded water, the intermediate one at 1619 cm^{-1} also belongs to coordinated water molecules but with a weaker coordination bond, and the band at 1597 cm^{-1} is attributed to water molecules with stronger interaction with Pb^{2+} cations [4].

After the complex was heated to 120 °C, the absorption bands due to coordinated and zeolitic water disappear. Only one broad band remains which can be assigned to humidity adsorbed on the KBr used to make the pellets. The FTIR spectrum of the dehydrated complex, $Pb_2[Fe(CN)_6]$, corresponds to an hexacyanometallate indicating that the dehydration process does not change the metal-cyano framework of the Pb^{+2} complex salt. The ν(C≡N) was not affected by the dehydration process. Gómez et al. [28] have reported that on dehydration of $Mn_2[Fe(CN)_6]\cdot 8H_2O$, the C≡N stretching bands shift to low frequencies, because in these conditions Mn increases its interaction with the C≡N ligands mainly through a σ-bonding mechanism. To compensate for that effect the C≡N ligands take more electrons from the Fe through a π back-bonding mechanism, weakening the C≡N bond. As a result of these combined effects the C≡N stretching vibration shift to lower frequency. This feature has not been observed in $Pb_2[Fe(CN)_6]$. Additionally, laboratory PXRD taken to this sample (see Fig. S1 in Supplementary information) is coincident with Powder Diffraction File # 48-0225 informed for anhydrous $Pb_2[Fe(CN)_6]$.

3.2. Crystal structure

The crystal structure of $Pb_2[Fe(CN)_6]\cdot 4H_2O$ was solved using SXRPD data. The pattern was indexed using the program DICVOL [22] with the first 25 diffraction peaks of the pattern. A monoclinic unit cell was found with high figures of merit $M(25) = 110$ and $F(25) = 509$. The possible space groups were reduced to eight from the extinction analysis: $P2_1/n$, Pn, $P2/n$, $P2_1$, $P2_1/m$, $P2/m$, Pm and $P2$. The unit cell parameters were refined using the Le Bail method [24]. All eight space groups were tried during the structure solution procedure using the direct methods and Patterson electron density maps calculated with the program SHELXS from extracted integrated intensities according to the Le Bail method [24]. The structure solution in the space group $P2_1/n$ produced an appropriate structural model. Then, this model was refined in order to obtain the atomic positions, thermal displacement parameters and occupation factors, and bond distances and angles. The hydration degree, estimated from the oxygen atom occupation factors of the water molecules (coordinated and zeolitic), agrees with the one derived from the TGA curves. Fig. 2 shows the experimental and fitted SPXRD patterns and their difference. The final values of the cell parameters and the details of the crystal structure refinement are summarized in Table 1. Table 2 contains the refined atomic positions, thermal displacement parameters and occupation factors. The interatomic distances and bond angles calculated are shown in Table 3. The inner cation Fe^{2+} is located on an inversion center and it has the usual octahedral coordination observed in hexacyanometallates (see Fig. S2 in Supplementary information). The most interesting characteristic of this structure is the penta-fold coordination of the Pb^{2+} cations (Fig. 3). The coordination polyhedron of Pb^{2+} (a distorted square pyramid) is formed by three N atoms from C≡N ligands and two O atoms from coordinated water. Two adjacent Pb^{2+} are linked by two aquo bridges. The formation of the aquo bridges leads to a high stabilization of the coordinated water [5]. The distorted square pyramid (an octahedra without one of its corners) around Pb^{2+} is compatible with

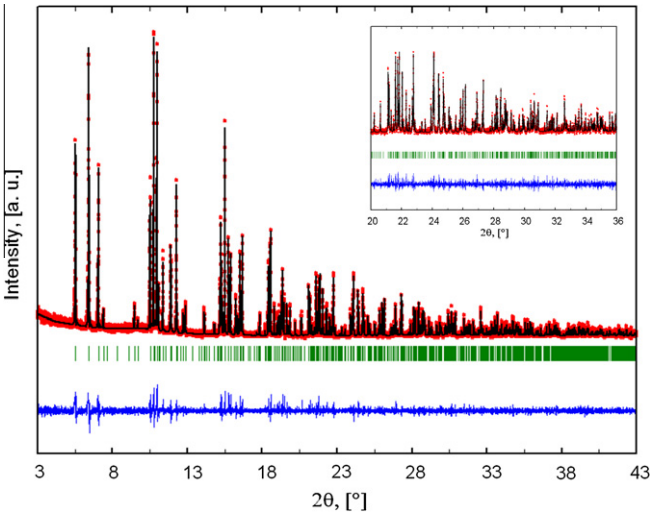

Fig. 2. SXRPD pattern observed (red), calculated (black) and difference curve (blue) for the Rietveld refinement of $Pb_2[Fe(CN)_6]\cdot 4H_2O$. The inset shows a zoom (5×) of the high angle region (Color online).

Table 1
Details of the refined crystal structure by the Rietveld method.

	$Pb_2[Fe(CN)_6]\cdot 4H_2O$
Data collection	
Diffractometer	synchrotron radiation
Wavelength (Å)	0.699204
2θ Range (°)	1.000–43.543
Step size (°)	0.003
Unit cell	
Space group	$P2_1/n$ [14]
Cell parameters (Å)	a = 10.9763(1)
	b = 7.6283(3)
	c = 8.5701(2)
	β = 98.84(6)°
V (Å^3)	709.04(7)
Z	2
Refinement	
Experimental points	14 182
Effective reflections	675
Constrain distances	6
Refined parameters	
Profile	11
Structural	37
Figures of merit	
Rexp	9.77
Rwp	17.4
RB	7.2
S	1.78

Table 2
Atomic parameters, thermal factors and of occupation for the refined crystal structure.

Composition	Site	x	x	z	Biso	Occ
$Pb_2[Fe(CN)_6]\cdot 4H_2O$						
Fe	2a	0	0	0	0.82(5)	1
Pb	4e	0.171(9)	0.0021(8)	0.6105(6)	1.19(2)	1
C1	4e	0.097(3)	−0.0053(9)	0.2033(6)	1.04(1)	1
N1	4e	0.160(9)	0.011(8)	0.3219(6)	1.04(1)	1
C2	4e	0.099(3)	0.186(1)	−0.056(2)	1.04(1)	1
N2	4e	0.1416(6)	0.308(8)	−0.102(5)	1.04(1)	1
C3	4e	0.1112(9)	−0.178(1)	−0.038(2)	1.04(1)	1
N3	4e	0.174(1)	−0.273(4)	−0.090(6)	1.04(1)	1
O1	4e	0.011(1)	−0.2814(9)	0.4896(7)	1.38(1)	1
O2	4e	0.0808(9)	0.498(7)	0.2859(7)	2.4(1)	1

Table 3
Main distances and bond angles for the refined crystal structure.

Composition	Bond distance (Å)				Bond angle (°)
$Pb_2[Fe(CN)_6]\cdot 4H_2O$	Fe–C1 = 1.89(9)	C1–N1 = 1.14(8)	Pb–N1 = 2.45(8)	Fe–C1–N1 = 171.4(8)	Pb–N1–C1 = 144.6(6)
	Fe–C2 = 1.89(6)	C2–N2 = 1.14(3)	Pb–N2 = 2.53(2)	Fe–C2–N2 = 168.9(2)	Pb–N2–C2 = 149.3(1)
	Fe–C3 = 1.88(8)	C3–N3 = 1.14(1)	Pb–N3 = 2.43(1)	Fe–C3–N3 = 166.6(6)	Pb–N3–C3 = 161.0(5)
			Pb–O1 = 2.88(2)		
			Pb–O1 = 2.96(3)		

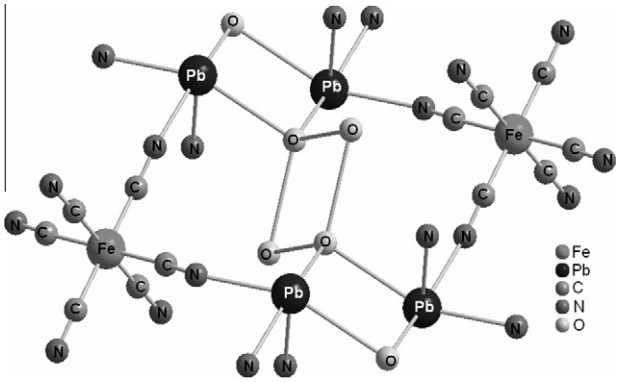

Fig. 3. Coordination environment of the Fe^{+2} and Pb^{+2} ions in $Pb_2[Fe(CN)_6]\cdot 4H_2O$. Pb^{+2} ions are penta-fold coordinated by three N atoms plus two water molecules, and Fe^{+2} is octahedrally coordinated by six C≡N groups forming the molecular block $[Fe(CN)_6]^{-4}$. A water molecule cluster is formed in the cavity between the metal centers.

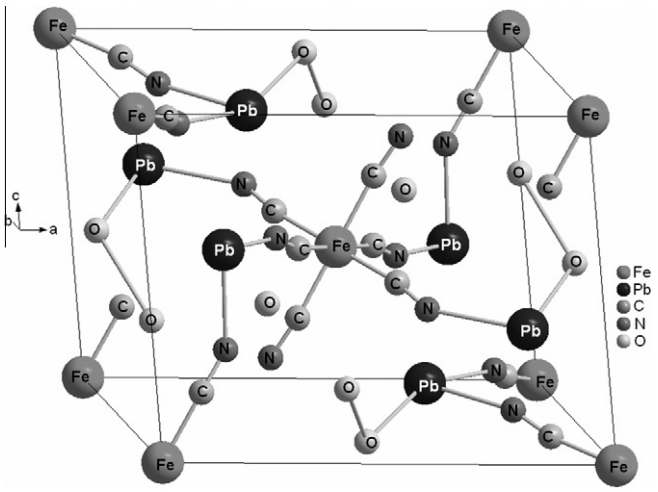

Fig. 4. Crystal packing within the unit cell and coordination environment for Fe^{+2} and Pb^{+2} in $Pb_2[Fe(CN)_6]\cdot 4H_2O$. Some water molecules of the unit cell were omitted for clarity.

the presence of its inert pair s^2 which should be pointing towards the absent corner of the octahedra. Fig. 4 shows the crystal packing within the unit cell and the coordination environment of the metal centers. The unusual Fe–C≡N–$Pb(H_2O)_2$–Pb–N≡C–Fe linkage alternates with the usual Pb–N≡C–Fe one (see Fig. S3 in Supplementary information). Zeolitic water molecules are also observed in the structure; they are located in small channels in the structure and they are hydrogen bonded to coordinated water molecules forming a cumulus. Coordinated water that link Pb^{2+} cations do not interact through hydrogen bonding, since they are very distant (at 3.35 Å) and their O atoms are ligands of Pb^{2+}.

The crystal structure of $Pb_2[Fe(CN)_6]\cdot 4H_2O$ is quite different to the one of anhydrous $Pb_2[Fe(CN)_6]$. The anhydrous complex crystallizes in the trigonal crystal system, space group $P\bar{3}$. The structure consists of infinite trigonal layers formed by $[Fe(CN)_6]^{4-}$ units. Fe^{2+} ions are located inside these complexes and coordinated to six C atoms from C≡N ligands. Pb^{2+} ions are positioned within distorted octahedra formed by six N atoms belonging to the six nearest $Fe(CN)_6$ complexes (three units from each one of two different layers). The interaction between $[Fe(CN)_6]^{4-}$ complexes occurs through N–Pb–N bonds [1], and there are three long and three short Pb–N interatomic distances (see Ref. [1]).

3.3. Thermal decomposition of $Pb_2[Fe(CN)_6]\cdot 4H_2O$

TGA and DTA data for $Pb_2[Fe(CN)_6]\cdot 4H_2O$ are shown in Fig. 5. The first weight loss step corresponds to the loss of four molecules of water (coordinated and zeolitic) to form the anhydrous phase that remains stable up to above 300 °C. The low dehydration temperature is due to the low polarizing power of the Pb^{2+} ion which consequently bonds weakly to its coordinated water molecules. Despite that there are two types of water molecules (coordinated and zeolitic), only one step of dehydration is observed. This is due to the fact that once zeolitic water molecules are eliminated, hydrogen bonds to the coordinated water molecules are broken, thus these water molecules become unstable because Pb^{2+} is a large ion with low polarizing power, and as a result coordinated molecules are eliminated together with the zeolitic ones.

The second step finishes at about 500 °C, and it corresponds to the elimination and oxidation of the cyanide groups with the simultaneous formation of simple oxides PbO and Fe_2O_3, which was corroborated by laboratory PXRD data (discussed below). See the large exothermic process in the DTA, characteristic of an oxidation process. In the last step at temperatures higher than 500 °C, the simple oxides react (without mass loss) to produce the mixed oxide $Pb_2Fe_2O_5$ and PbO (also confirmed by PXRD data). The sequence of decomposition steps can be expressed as:

$$Pb_2[Fe(CN)_6]\cdot 4H_2O_{(s)} \rightarrow Pb_2[Fe(CN)_6]_{(s)} + 4H_2O_{(g)} \quad (1)$$

$$Pb_2[Fe(CN)_6]_{(s)} + \frac{55}{4}O_{2_{(g)}} \rightarrow \frac{1}{2}Fe_2O_{3_{(s)}} + 2PbO_{(s)} + 6CO_{2_{(g)}} + 6NO_{2_{(g)}} \quad (2)$$

$$\frac{1}{2}Fe_2O_{3_{(s)}} + 2PbO_{(s)} \rightarrow \frac{1}{2}Pb_2Fe_2O_{5_{(s)}} + PbO_{(s)} \quad (3)$$

The gas products (CO_2 and NO_2) are rather speculative, but they are expected to be the oxidation products of the cyanides in an air atmosphere. It has been shown experimentally that the decomposition of hexacyanometallates in an inert atmosphere produces the intermediate C_2N_2 [29], but in our conditions this will be rapidly oxidized to CO_2 and NO_2. In fact solid reactants and products are important in order to explain TGA data. The mass losses expected in each of the decomposition steps are in good agreement with those calculated from the TGA curve (shown in Table S1 of the Supplementary information). The nature of the solid residues obtained

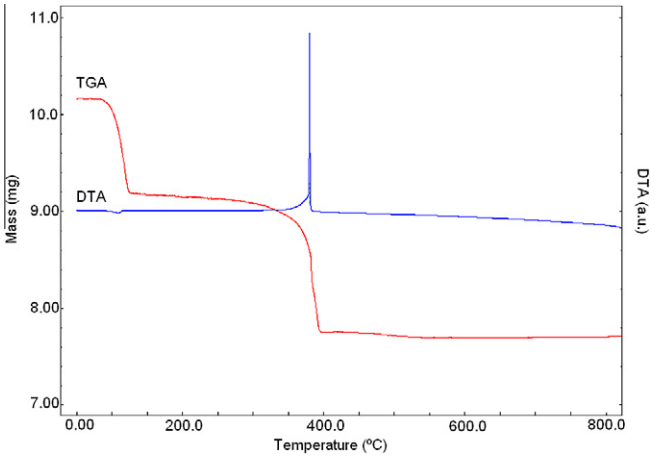

Fig. 5. TG and DTA curve of $Pb_2[Fe(CN)_6]\cdot 4H_2O$ in air at 5 °C/min.

in the last stage of the thermal decomposition process has been confirmed from laboratory PXRD and FTIR. The total mass loss from RT to 500 °C is 24.28% in agreement with the theoretical mass loss (24.65%) for the formation of $Pb_2Fe_2O_5$ and PbO from the complex. The DTA curve shows an endothermic peak at 87 °C due to the dehydration process. The second exothermic peak located at 373 °C corresponds to the elimination and oxidation of the cyanide groups.

3.4. Thermal treatments of $Pb_2[Fe(CN)_6]\cdot 4H_2O$

In order to analyze the oxides obtained after thermal decomposition in air atmosphere at different temperatures, the resulting products at each stage were characterized by laboratory PXRD (Fig. 6). The composition of the residues at different temperatures was determined using the X'Pert Highscore Program (version 2.1b, PANalytical, B.V. Almelo, The Netherlands). When the complex was heated at 500 °C, some peaks attributed to PbO (PDF # 072-0093) and Fe_2O_3 (PDF # 40-1139) were observed, showing an incomplete reaction. When the complex was decomposed at temperatures higher than 650 °C, the PXRD analysis showed the pattern corresponding to $Pb_2Fe_2O_5$ (PDF # 33-0756) and PbO (PDF # 072-0093). The diffraction peaks of PbO always appeared in the PXRD pattern of the thermal decomposition products because the chemical ratio of Pb:Fe is 2:1 and exceeds the one needed for the formation of $Pb_2Fe_2O_5$. The JCPD card assigns a tetragonal structure to $Pb_2Fe_2O_5$; however Abakumov et al. had recently identified $Pb_2Fe_2O_5$ to be a monoclinic structure by careful analysis of HRTEM images and electron diffraction patterns [19]. The preparation of $Pb_2Fe_2O_5$ in a single phase appears to be a difficult problem. It has been reported that the chemical compositions of the crystallographic shear (CS) structures found in the $Pb_2Fe_2O_5$ sample correspond to the formula $Pb_{0.9375}FeO_{2.4375}$, $Pb_{0.9}FeO_{2.4}$ and $Pb_{0.875}FeO_{2.375}$ [30]. All these compositions correspond to the general formula of $Pb_2Fe_2O_5\cdot xPbO$, where $x = 0.0625$, 0.1 and 0.125 [30]. $Pb_2Fe_2O_5$ is expected to be an anion-deficient perovskite and it adopts a crystallographic shear planes structure with alternating layers of FeO_5 pyramids and FeO_6 octahedra [19]. Because of the complexity of the structure and the prevalence of domain fragmentation, this material is not well understood.

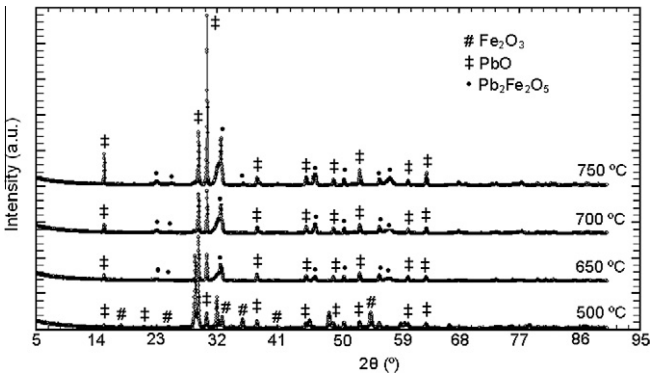

Fig. 6. Laboratory PXRD data of samples obtained by thermal decomposition of $Pb_2[Fe(CN)_6]\cdot 4H_2O$ at 500 °C, 650 °C, 700 °C, and 750 °C.

FTIR spectra of the samples obtained by thermal decomposition of $Pb_2[Fe(CN)_6]\cdot 4H_2O$ at different temperatures showed that the $\nu(C{\equiv}N)$ stretching band disappeared when the complex was heated at 500 °C, and bands attributable to carbonate groups in 1500–1100 cm^{-1} range began to appear (Fig. S4 in Supplementary information). When the complex was heated to 650 °C, the bands corresponding to carbonate groups disappeared and only a strong band for the stretching M–O typical of oxides was observed at 561 cm^{-1}. This situation did not change at temperatures higher than 650 °C [27]. The broad band observed in all the samples in the 3700–3100 cm^{-1} range corresponds to the surface-adsorbed water and oxygen species after calcinations. The bands corresponding to water and CO_2 chemisorbed on the surface, are observed because these materials have a high surface area. The fact that they are only at the surface is shown by its absence in the PXRD data for all the products. Similar results were obtained by some of us for $YFeO_3$ prepared by thermal decomposition of $Y[Fe(CN)_6]\cdot 4H_2O$ [8] and $AFeO_{3-\delta}$ (A = alkaline earth) prepared by thermal decomposition of alkaline earth nitroprussides [10,11]. However, in the case of A = Ba, $BaCO_3$ was observed in the PXRD data, indicating the presence of bulk $BaCO_3$. This difference must be assigned to the highest stability of $BaCO_3$ compared with all other carbonates.

The size and morphologies of $Pb_2[Fe(CN)_6]\cdot 4H_2O$ and its decomposition products were investigated by SEM. The SEM micrograph of $Pb_2[Fe(CN)_6]\cdot 4H_2O$ powder (Fig. S5 in Supplementary information) shows that it is composed of well-defined crystals with plate shapes and around 3 μm size. The SEM photograph of $Pb_2Fe_2O_5$ obtained at 700 °C clearly shows that the shape and morphology is quite different to the one of its precursor complex. The crystals of the precursor were completely disrupted and fine particles of the order of 1.3 μm appeared.

4. Conclusions

The crystal structure of $Pb_2[Fe(CN)_6]\cdot 4H_2O$ was solved and refined from SPXRD. This compound crystallizes in the monoclinic crystal system, space group $P2_1/n$ and $Z = 2$. In this structure the Fe^{2+} ion is octahedrally coordinated to six cyano groups and the Pb^{2+} ion is penta-fold coordinated to three N atoms from $C{\equiv}N$ ligands and two O from coordinated water molecules. The most important peculiarity of the structure of this complex is the occurrence of water bridges linking two neighboring Pb^{2+} cations. An unusual $Fe{-}C{\equiv}N{-}Pb(H_2O)_2{-}Pb{-}N{\equiv}C{-}Fe$ linkage alternates with a usual $Pb{-}N{\equiv}C{-}Fe$ one. Zeolitic water molecules are also observed in the structure; they are located in small channels in the structure and they are hydrogen bonded to coordinated water molecules forming a cumulus. Coordinated and zeolitic water molecules can be removed without affecting the hexacyanometallate framework.

The thermal decomposition of $Pb_2[Fe(CN)_6]\cdot 4H_2O$ in air was studied using TGA/DTA analysis. It decomposes in three steps. The first one corresponds to the elimination of four water molecules, the second one to the cyanide elimination by combustion

to give Fe_2O_3 and PbO, and finally in the third step (without mass loss) the simple oxides react to produce the mixed oxide $Pb_2Fe_2O_5$ and PbO.

The mixed oxide $Pb_2Fe_2O_5$ is an anion-deficient perovskite and it adopts a crystallographic shear planes structure with alternating layers of FeO_5 pyramids and FeO_6 octahedra. $Pb_2Fe_2O_5$ is a multiferroic candidate, which could open a new field of research for complex oxides with multiferroic properties.

Acknowledgments

R.E.C. thanks FONCYT for PICT2007 303, CONICET for PIP #11220090100995 and SECyT-UNC for the Proyect 159/09. D.M.G. thanks CONICET for a fellowship. D.M.G and M.I.G. thank CIUNT for financial support. M.A. and E.R. thank the support provided by the Project SEP-CONACyT-2009-01-129048. Use of the National Synchrotron Light Source, Brookhaven National Laboratory, was supported by the US Department of Energy, Office of Science, Office of Basic Energy Sciences, under Contract No. DE-AC02-98CH10886.

Appendix A. Supplementary data

Structural information derived from the crystal structure refinement of $Pb_2[Fe(CN)_6]\cdot 4H_2O$ has been deposited at the ICSD Fachinformationszentrum Karlsruhe (FIZ) (E-mail: CrysDATA@FIZ.Karlsruhe.DE) with ICSD File No. 423224. Supplementary data associated with this article can be found, in the online version, at doi:10.1016/j.poly.2011.12.006.

References

[1] V.G. Zubkov, A.P. Tyutyunnik, I.F. Berger, L.G. Maksimova, T.A. Denisova, E.V. Polyakov, I.G. Kaplan, V.I. Voronin, Solid State Sci. 3 (2001) 361.
[2] A.G. Sharpe, The Chemistry of the Cyano Complexes of the Transition Metals, Academic Press, London, 1976.
[3] J. Rodriguez Hernández, A. Gómez, E. Reguera, J. Phys. D: Appl. Phys. 40 (2007) 6076.
[4] M. Avila, L. Reguera, J. Rodriguez-Hernandez, J. Balmaseda, E. Reguera, J. Solid State Chem. 181 (2008) 2899.
[5] R. Martinez García, L. Reguera, M. Knobel, E. Reguera, J. Phys.: Condens. Matter 19 (2007) 1.
[6] V.M. Zainullina, M.A. Korotin, L.G. Maksimova, Phys. Solid State 46 (2004) 1836.
[7] M.C. Navarro, E.V. Pannunzio-Miner, S. Pagola, M.I. Gómez, R.E. Carbonio, J. Solid State Chem. 178 (2005) 847.
[8] D.M. Gil, M.C. Navarro, M.C. Lagarrigue, J. Guimpel, R.E. Carbonio, M.I. Gómez, J. Therm. Anal. Calorim. 103 (2011) 889.
[9] M.C. Navarro, M.C. Lagarrigue, J.M. De Paoli, R.E. Carbonio, M.I. Gómez, J. Therm. Anal. Calorim. 102 (2010) 655.
[10] M.I. Gómez, J.A. de Morán, R.E. Carbonio, P.J. Aymonino, J. Solid State Chem. 142 (1999) 138.
[11] M.I. Gómez, G. Lucotti, J.A. Morán, P.J. Aymonino, S. Pagola, P. Stephens, R.E. Carbonio, J. Solid State Chem. 160 (2001) 17.
[12] Y. Itagaki, M. Mori, Y. Hosoya, H. Aono, Y. Sadaoka, Sens. Actuators B 122 (2007) 315.
[13] R.E. Cohen, Nature 358 (1992) 136.
[14] A. Moreira dos Santos, S. Parashar, A. Raju, Y.S. Zhao, A.K. Cheetham, C.N.R. Rao, Solid State Commun. 122 (2002) 49.
[15] P.S. Halasyamani, Chem. Mater. 16 (2004) 3586.
[16] D.I. Khomskii, J. Magn. Magn. Mater. 306 (2006) 1.
[17] A.A. Belik, N. Tsujii, H. Suzuki, E. Takayama-Muromachi, Inorg. Chem. 46 (2007) 8746.
[18] K.Y. Yun, M. Noda, M. Okuyama, J. Appl. Phys. 96 (2004) 3399.
[19] A.M. Abakumov, J. Hadermann, S. Bals, I.V. Nikolaev, E.V. Antipov, G. Van Tendeloo, Angew. Chem., Int. Ed. 45 (2006) 6697.
[20] J. Hadermann, A.M. Abakumov, I.V. Nikolaev, E.V. Antipov, G. Van Tendeloo, Solid State Sci. 10 (2008) 382.
[21] M. Wang, G. Tan, Mater. Res. Bull. 46 (2011) 438.
[22] L. Lower, R. Vargas, J. Appl. Crystallogr. 15 (1982) 542.
[23] G.M. Sheldrick, Program for Crystal Structure Determination, Institute fur Anorg. Chemie, Göttingen, Germany, 1997.
[24] A.L. Le Bail, Mater. Sci. Forum 378–381 (2001) 65.
[25] R.A. Young, The Rietveld Method, Oxford University Press, New York, 1995.
[26] J. Rodríguez Carbajal, Physica B 192 (1993) 55.
[27] K. Nakamoto, Infrared and Raman Spectra of Inorganic and Coordination Compounds, Wiley, New York, 1986.
[28] A. Gómez, V.H. Lara, P. Bosch, E. Reguera, Powder Diffr. 17 (2002) 144.
[29] M.M. Chamberlain, A.F. Greene Jr., J. Inorg. Nucl. Chem. 25 (1963) 1471.
[30] A.M. Abakumov, J. Hadermann, G. Van Tendeloo, E.V. Antipov, J. Am. Ceram. Soc. 91 (2008) 1807.